LT-STM studies on substrate-dependent self-assembly of small organic molecules

2011 J. Phys. D: Appl. Phys. 44 464005

(http://iopscience.iop.org/0022-3727/44/46/464005)

IOP PUBLISHING JOURNAL OF PHYSICS D: APPLIED PHYSICS

J. Phys. D: Appl. Phys. **44** (2011) 464005 (13pp) doi:10.1088/0022-3727/44/46/464005

LT-STM studies on substrate-dependent self-assembly of small organic molecules

Han Huang[1], Swee Liang Wong[1,2], Wei Chen[1,3] and Andrew Thye Shen Wee[1]

[1] Department of Physics, National University of Singapore, 2 Science Drive 3, Singapore 117542, Singapore

[2] NUS Graduate School for Integrative Sciences and Engineering, National University of Singapore, 28 Medical Drive, Singapore 117456, Singapore

[3] Department of Chemistry, National University of Singapore, 3 Science Drive 3, Singapore 117543, Singapore

E-mail: phyhh@nus.edu.sg (H Huang) and phyweets@nus.edu.sg (A T S Wee)

Received 9 May 2011, in final form 21 July 2011
Published 4 November 2011
Online at stacks.iop.org/JPhysD/44/464005

Abstract

Low temperature scanning tunnelling microscopy is widely used to image and manipulate individual atoms and molecules on surfaces, as well as to investigate surface molecular processes such as diffusion, desorption, and configuration switching, at the atomic scale. The aim of this contribution is to highlight our recent progress in understanding the interface between small organic molecules and different substrates, focusing on two model systems: copper hexadecafluorophthalocyanine ($F_{16}CuPc$) on HOPG, Ag(1 1 1), Bi/Ag(1 1 1), and copper(II) phthalocyanine (CuPc) on perylene-3,4,9,10-tetracarboxylic-3,4,9,10-dianhydride (PTCDA) and C_{60} pre-covered surfaces. The influence of the underlying substrates on the molecular packing is discussed.

(Some figures in this article are in colour only in the electronic version)

1. Introduction

Over the past decades, thin-film based organic electronic devices have attracted much attention due to their potential applications in low-cost, large-scale and flexible electronic devices [1–10]. Significant developments in performance have been achieved for organic light-emitting diodes (OLEDs), organic field-effect transistors (OFETs), organic photovoltaic cells (OPVs) and organic spintronics [11]. Many investigations have been devoted to understanding electronic structures at organic/inorganic or organic/organic interfaces [12–16], and engineering interface properties through various surface modification schemes to enhance device performance [17–21]. It is found that the molecular packing of the first few organic layers at the interface plays crucial roles in determining the charge carrier transport and injection as well as molecular magnetism. For instance, a high hole mobility close to $10\,cm^2\,V^{-1}\,s^{-1}$ can be achieved in titanyl phthalocyanine (TiOPc)-based thin-film transistors due to close intermolecular π–π contact [22]. Recently, the topic of single-molecule magnets has become increasingly popular. Controlling the spin of a single molecule can be realized by manipulating the adsorbed molecule configuration [23–26] or by a chemical stimulus [27–30]. As such, the understanding and tailoring of the supramolecular packing and adsorption configurations at the molecular level are important for the optimization and performance of organic devices.

The growth behaviours [31–33] of organic molecules on inorganic substrates such as adsorption, desorption, diffusion, growth and nucleation, as shown in figure 1, are dominated by the delicate balance between molecule–substrate interfacial interactions and intermolecular interactions [34–44]. Most planar organic molecules lie flat on metallic substrates due to the effective overlapping between the substrate electronic states and the π-orbitals in molecules [43]; but they are found to adsorb in a 'standing-up' configuration on surfaces such as SiO_2 due to weak molecule–substrate interfacial interactions [44]. In particular, the interfacial interactions on noble metal surfaces are intermediate in strength, and stem from weak chemisorption and van der Waals (vdW) forces. On such surfaces, some organic molecules, such as metal-free phthalocyanine (H_2Pc) [45], CuPc [46–48], FePc [23, 49], perylene [50] form a 2D gas phase in the submonolayer regime due to intermolecular repulsive interactions; other molecules

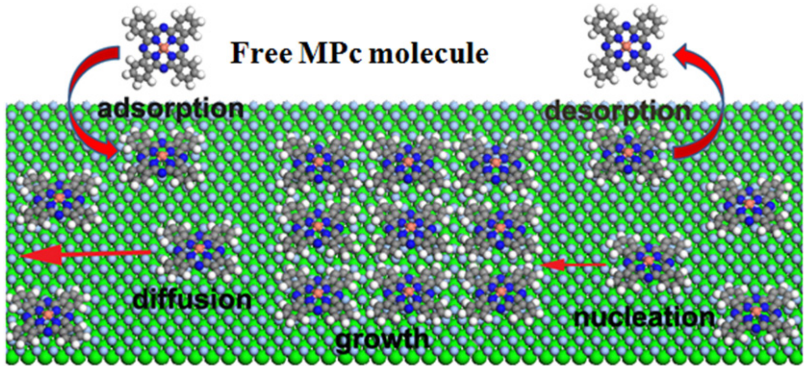

Figure 1. Schematic drawing of processes relevant in organic thin-film growth on metal surface, such as adsorption, desorption, diffusion, nucleation and growth of islands. The MPc molecular structure is also shown.

form 2D single-layered islands due to intermolecular attractive interactions, such as perylene-3,4,9,10-tetracarboxylic-3,4,9,10-dianhydride (PTCDA) on noble metal surfaces [51–55] and tetra(4-bromophenyl)porphyrin on Au(1 1 1) [56]. Due to the different inherent properties of organic materials, i.e. large size, anisotropy and relatively weak non-covalent intermolecular interactions, a comprehensive understanding of the organic–inorganic interface is still lacking.

Due to their chemical-, thermal- and air-stability, the family of phthalocyanines (Pcs), such as H_2Pc, metal phthalocyanines (MPcs, figure 1) and their derivatives, has been extensively applied in OLEDs [57], OFETs [58], OPVs [59] chemical sensors [60] and organic spintronics [61]. Both the electrical and optical properties of Pcs can be tuned by modifying their chemical structures. Films of various MPcs have been studied in the recent literature [39, 62–64]. Copper hexadecafluorophthalocyanine ($F_{16}CuPc$) represents a promising n-type semiconducting molecule for use in organic semiconductor devices, in particular in n-channel and bipolar OFETs [65–69]. Previous studies on $F_{16}CuPc$ on inert dielectrics such as SiO_2, reveal that $F_{16}CuPc$ molecules adopt a standing-up configuration with their molecular π-plane oriented nearly perpendicular to the substrate surface [70–72]. Scanning tunnelling microcopy (STM) is a powerful tool to study molecule packing and configurations at the (sub)molecular level due to its high lateral resolution [73–77]. In this contribution, we will review the low temperature (LT) STM investigation of the growth behaviours of the 1st and 2nd monolayer (hereafter ML) $F_{16}CuPc$ on model Bi/Ag(1 1 1) system (namely the metallic Ag(1 1 1), Ag(1 1 1)-$\sqrt{3} \times \sqrt{3}$R30°-Bi surface alloy (hereafter, Bi-$\sqrt{3}$), semimetal Bi-$P \times \sqrt{3}$ overlayer on Ag(1 1 1) and Bi(1 1 0) monolayer on Ag(1 1 1) [78–81][4] and on HOPG [82] to understand the effect of molecule–substrate interfacial interactions on molecular arrangement. In comparison, the growth of CuPc on PTCDA [83] and C_{60} [84] pre-covered surfaces is also briefly introduced.

[4] The model Bi/Ag(111) system can transform into surface phases with different geometric and electronic structures depending on the Bi coverage.

2. Monolayer F_{16}CuPc on different solid substrates

2.1. F_{16}CuPc on Ag(1 1 1)

At the initial growth stage, $F_{16}CuPc$ molecules predominantly decorate Ag(1 1 1) step edges, assembling into single-molecular chains with the molecular plane bridging over the edges, indicating appreciable molecular diffusion at room temperature (RT) and energetically favourable adsorption at step edges. Upon saturation of the edges, $F_{16}CuPc$ molecules nucleate into monolayer islands with irregular shapes on terraces, indicating attractive intermolecular interactions. The supramolecular packing is retained until the 1st ML completion, suggesting that the growth is dominated by intermolecular attraction. This contrasts with the case of the 1st ML CuPc on Ag(1 1 1) where intermolecular repulsion dominates the growth [47]. Figure 2(*a*) shows a single domain of such a structure. While $F_{16}CuPc$ molecules arrange in wave-like features along [1–10], the nearest neighbour (NN) direction on Ag(1 1 1), they form well-ordered interdigitated one-dimensional (1D) molecular chains along [1–21], the next nearest neighbour (NNN) direction with equal inter-chain separations (within experimental error). The corresponding fast Fourier transform (FFT) image inserted in figure 2(*a*) displays features of both equally spaced streaks parallel to the NNN directions and sharp diffraction spots along the NNN directions. While the intense spots are deduced from the equally spaced 1D $F_{16}CuPc$ molecular chains, and the streaks are led by the statistical distribution of intermolecular separations between $F_{16}CuPc$ molecules in neighbouring chains. Similar 1D molecular packing has been observed for Pcs on InSb(1 0 0)4 $\times$ 2/c(8 $\times$ 2) [39, 85–87].

The LEED pattern of 1 ML $F_{16}CuPc$ on Ag(1 1 1) is shown in figure 2(*b*) (primary beam energy of 12 eV), where spot (0, 0) and the [1 −1 0] direction of Ag(1 1 1) are indicated. The integral diffraction spots of Ag(1 1 1) are invisible because the primary beam energy is low. Taking the 3-fold symmetry of the substrate into account, the above-mentioned FFT pattern is in good agreement with the LEED pattern. Clearly, the 1D chains are directed along the crystallographic axes of Ag(1 1 1). Otherwise, the LEED pattern will be more complex due to mirror symmetry about the crystallographic axes [88]. The corresponding schematic of the LEED pattern is shown in

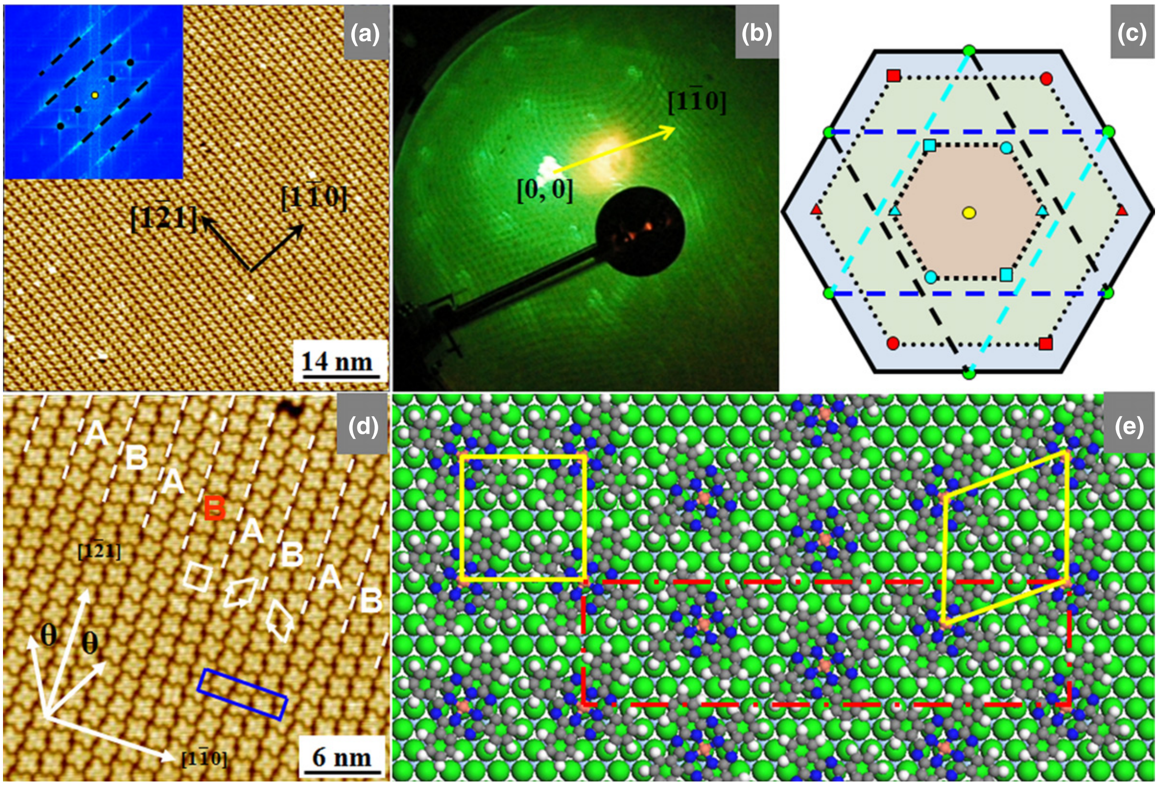

Figure 2. The 1st ML F_{16}CuPc on Ag(1 1 1). (*a*) STM image ($V_T = 1.90$ V, $I_T = 0.1$ nA) showing single domain of F_{16}CuPc on Ag(1 1 1). The corresponding FFT is shown as an inset. (*b*) The LEED pattern of 1 ML F_{16}CuPc on Ag(1 1 1) at 12 eV and (*c*) the corresponding schematic LEED pattern. The three equivalent domains are marked by different symbols. (*d*) Molecularly resolved STM image ($V_T = 1.90$ V, $I_T = 0.1$ nA) of 1 ML F_{16}CuPc on Ag(1 1 1). The azimuths of the substrate are shown by the set of arrows. θ is the smaller azimuthal angle between molecular diagonals and the molecular chain direction. Three unit cells are highlighted by three white tetragons, respectively. The blue rectangle highlights one unit cell of the super herringbone structure. Different domains are separated by dashed lines and labelled 'A' and 'B'. (*e*) Proposed models of F_{16}CuPc on Ag(1 1 1). (Figure (*d*) amended and reprinted with permission from [80], copyright (2008) by the American Chemical Society.)

figure 2(*c*). Except for the three sets of hexagonal diffraction spots (in different colours), streaks can also be observed in the LEED pattern in the NNN directions of Ag(1 1 1), marked by dashed lines. The red spots are the 2nd order diffraction of those cyan ones, in the NNN directions. The spots indicated by different symbols are incoherent and from different domains caused by the 3-fold symmetry of the substrate. The green ones are located at the intersection points of the 1st and 2nd order streaks. Within experimental errors, one green spot is located at (1/3, 0), which reveals that the intermolecular distance in the 1D molecular chain is $3\sqrt{3}\boldsymbol{d} = 15.02$ Å, where $\boldsymbol{d} = 2.89$ Å, the lattice constant of Ag(1 1 1). It is difficult to determine the exact inter-chain separation from the LEED pattern.

A higher resolution STM image of 1 ML F_{16}CuPc on Ag(1 1 1) is shown in figure 2(*d*). Similar to other Pcs [89, 90], the four 'leaves' are assigned to the four F-substituted peripheral benzene rings and the centre dark hole to the Cu atom. F_{16}CuPc adopts a lying-down configuration with its molecular π-plane parallel to the surface, arising from the effective coupling between Ag d-band electrons and the π-orbitals in F_{16}CuPc. The in-plane orientation of the molecules in each chain is uniform with an intermolecular distance of $\boldsymbol{a} = 15.2 \pm 0.5$ Å, in consistence with the LEED results. The interdigitated 1D molecular chains are structurally different with the side-by-side 1D chains of PbPc on InSb [85, 86], but similar to that of submonolayer CoPc on Cu(1 1 1) [91]. This is attributed to the symmetry reduction (from C_4 to C_2) induced by the 3-fold symmetric substrates, which leads to easier molecular dimerization between two Pc molecules via two lobes along the NN directions [91]. The average inter-chain separation is measured to be 15.0 ± 0.5 Å. The two lengths are also consistent with the vdW dimensions of isolated F_{16}CuPc molecules [71, 92]. Combining the LEED with STM measurements, the inter-chain separation is determined to be $5\boldsymbol{d}$. Close inspection reveals that the molecules in two neighbouring molecular chains adopt the same in-plane orientation, and is referred to as a double-molecule-chain (DMC). Two types of DMCs alternatively appear and dominate the surface, and are labelled 'A' and 'B' in figure 2(*d*). For convenience, the smaller azimuthal angle between molecular diagonals and the molecular chain direction is defined as θ, indicated in figure 2(*d*), which is measured to be $30 \pm 2°$. One diagonal of the square molecule in DMC B is aligned along the [1 0 −1] direction of Ag(1 1 1); while one diagonal of the molecule in DMC A is along the [0 1 −1] direction, as indicated by a set of arrows in the lower-left corner in figure 2(*d*), which confirms $\theta = 30 \pm 2°$. This suggests that on terraces all F_{16}CuPc molecules have the same adsorption configuration with respect to the Ag(1 1 1) substrate, indicating

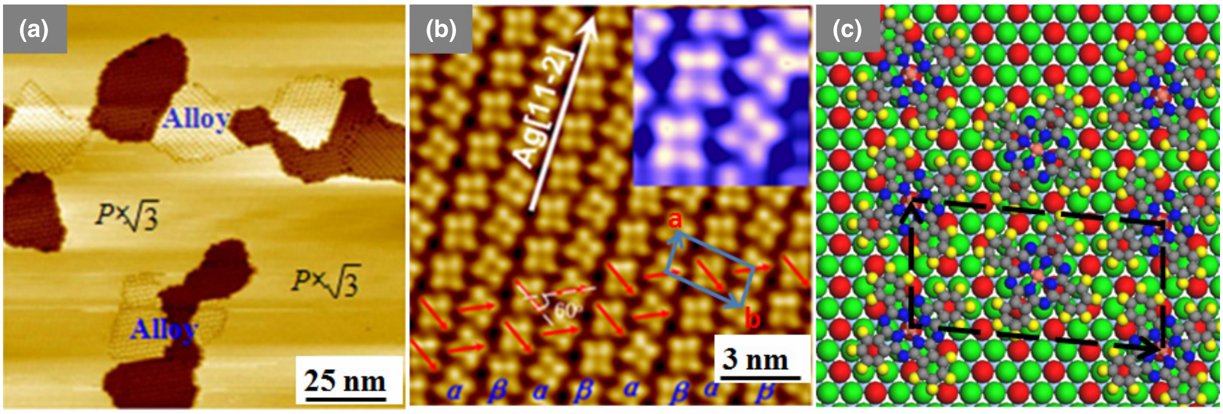

Figure 3. The 1st ML $F_{16}CuPc$ on Bi/Ag(1 1 1). (*a*) STM image ($V_T = 2.59$ V, $I_T = 0.1$ nA) of 0.2 ML $F_{16}CuPc$ deposited on the surface with co-existence of Bi-$\sqrt{3}$ and Bi-$P \times \sqrt{3}$, showing that $F_{16}CuPc$ molecules exclusively adsorb on Bi-$\sqrt{3}$. (*b*) Molecularly resolved STM image ($V_T = 2.87$ V, $I_T = 0.1$ nA) of one ML $F_{16}CuPc$ adsorbing on Bi-$\sqrt{3}$ and (*c*) the proposed model (red ball: bismuth; green ball: silver). One unit cell is highlighted in panels (*b*) and (*c*), respectively. (Figures (*a*) and (*b*) reprinted with permission from [81], copyright (2010) by the American Chemical Society.)

a good epitaxial relationship between $F_{16}CuPc$ and Ag(1 1 1). The two alternating adsorption configurations are believed to minimize the repulsion between molecular lobs along the NNN direction, where interaction between the lobs and substrate is stronger [91].

On the basis of the relative longitudinal translation in the molecular chain direction, two kinds of commensurate unit cells were proposed to describe the DMC, as shown by a square and a parallelogram in the proposed model in figure 2(*e*), denoted by the followed matrices: I$\begin{pmatrix} 5 & 0 \\ 3 & 6 \end{pmatrix}$, II$\begin{pmatrix} 6 & 2 \\ 3 & 6 \end{pmatrix}$, respectively. Both unit cells have the same footprint of around 216.4 Å^2, comparable to that of an isolated $F_{16}CuPc$ molecule of about 210 Å^2 [71, 92]. As highlighted by the white square in figure 2(*d*), a DMC labelled by a red 'B' has a square unit cell, corresponding to a type I unit cell. The other DMCs in figure 2(*d*), labelled by white 'A' and 'B', have the same oblique unit cells, as highlighted by the two equivalent parallelograms. They correspond to the type II unit cell. It is worth noting that the DMCs A and B are mirrored structures with a small lateral displacement. Therefore, it is not a simple mirror symmetry but a glide mirror symmetry in the first $F_{16}CuPc$ layer on Ag(1 1 1). One super unit cell comprising four $F_{16}CuPc$ molecules is highlighted by a blue rectangle, revealing a super herringbone structure described by a matrix of $\begin{pmatrix} 20 & 0 \\ 3 & 6 \end{pmatrix}$ with a 2D space group of *p*2*gg*. A unit cell of such a super herringbone structure is also highlighted in the proposed model in figure 2(*e*) by a dashed red rectangle. Type I DMC acts as a domain boundary in such super herringbone structure.

2.2. $F_{16}CuPc$ on Bi-$\sqrt{3}$

Figure 3(*a*) shows 0.2 ML $F_{16}CuPc$ deposited on a surface with co-existence of Bi-$\sqrt{3}$ and Bi-$P \times \sqrt{3}$ on Ag(1 1 1), where $F_{16}CuPc$ molecules exclusively adsorb on the Bi-$\sqrt{3}$ regions. It is found that the adsorption of $F_{16}CuPc$ on Bi-$P \times \sqrt{3}$ only happens after the Bi-$\sqrt{3}$ regions are fully saturated by $F_{16}CuPc$, indicating a stronger molecule–substrate interfacial interaction on Bi-$\sqrt{3}$ than on Bi-$P \times \sqrt{3}$. The molecularly resolved STM image in figure 3(*b*) shows that $F_{16}CuPc$ forms 1D molecular chains along the [1 1 −2] direction of Ag(1 1 1) with its molecular π-plane parallel to the surface, similar to the case on Ag(1 1 1). Careful inspection reveals that $F_{16}CuPc$ molecules in alternative chains adopt the same adsorption configuration, marked 'α' and 'β', respectively. An oblique unit cell comprising two molecules with parameters of $a = 14.5 \pm 0.5$ Å, $b = 30 \pm 1$ Å and $\gamma = 95 \pm 3°$ is highlighted in figure 3(*b*), where *a*-axis is oriented along the [1 1 −2] direction. Figure 3(*c*) shows the proposed model based on geometrical considerations, where the unit cell parameters are $a = 15.0$ Å, $b = 30.4$ Å and $\gamma = 95.3°$. Such a unit cell can be described by the matrix $\begin{pmatrix} 10 & -1 \\ 3 & 6 \end{pmatrix}$. One diagonal of $F_{16}CuPc$ is aligned along the NN directions of Ag(1 1 1), the other one diagonal is along the NNN direction. The two $F_{16}CuPc$ molecules in one unit cell are rotated ~60° with respect to each other, reflecting the 3-fold symmetry of underlying substrate. The smaller azimuthal angle between one molecular diagonal and the molecular chain direction, θ, is $30 \pm 2°$ for both configurations. Unlike on Ag(1 1 1), the adsorption sites of the two $F_{16}CuPc$ molecules in one unit cell are at non-equivalent sites: while one adsorbs at the Bi atop site, the other one adsorbs at the bridge site of two neighbouring Ag atoms, as shown in figure 3(*c*), confirming a weaker molecule–substrate interaction than that on Ag(1 1 1).

2.3. $F_{16}CuPc$ on other 3-fold symmetric substrates

The molecularly resolved STM images in figure 4 display 1 ML $F_{16}CuPc$ on (a) HOPG [82], (b) epitaxial graphene (EG) on SiC(0 0 0 1) [93], (c) Cu(1 1 1) [94] and (d) Au(1 1 1) [95], respectively. $F_{16}CuPc$ molecules lie flat with their molecular planes parallel to substrates. In figure 4(*a*), the indicated unit cell comprising two $F_{16}CuPc$ molecules with discrete azimuthal orientations (α and β) is oblique with parameters of $a = 15.5 \pm 0.5$ Å, $b = 31.0 \pm 0.5$ Å and $\gamma = 70 \pm 3°$. Along the *a*-axis direction, the molecules possess the same

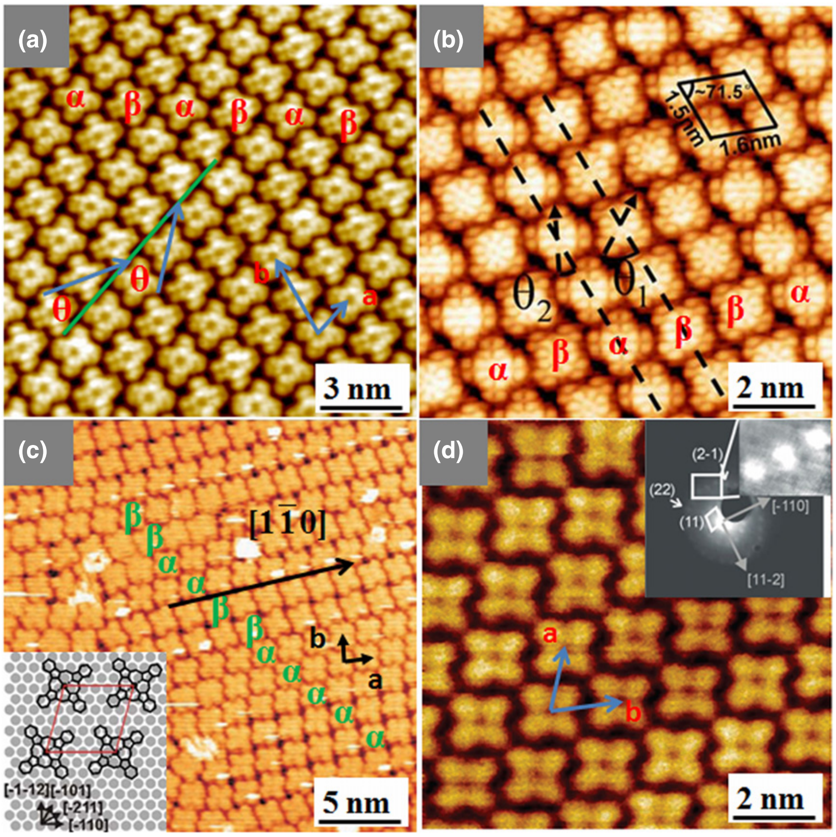

Figure 4. STM images of 1 ML $F_{16}CuPc$ (*a*) ($V_T = 2.00$ V, $I_T = 0.1$ nA) on HOPG, (*b*) ($V_T = 1.50$ V, $I_T = 0.1$ nA) on epitaxial graphene on SiC(0001), (*c*) on Cu(1 1 1) and (*d*) on Au(1 1 1). The inset in panel (*c*) is the proposed model. The inset in panel (*d*) is the corresponding LEED pattern. One unit cell is indicated in each panel, respectively. (Figure (*a*) reprinted with permission from [82], copyright (2009) by Springer; figure (*b*) reprinted with permission from [93], copyright (2010) by American Physical Society; figure (*c*) reprinted with permission from [94a], copyright (2007) by Wiley; figure (*d*) and the model in figure (*c*) reprinted with permission from [96], copyright (2010) by American Institute of Physics; the LEED pattern inserted in figure (*d*) reprinted with permission from [97], copyright(2009) by Wiley.)

in-plane orientation to form 1D molecular chains. Unlike on Ag(1 1 1) or Bi-$\sqrt{3}$, the molecular chains in configurations α and β appear randomly. Consecutive α or β chains can be usually observed on HOPG, where the unit cell parameters are $a = 15.5 \pm 0.5$ Å, $b = 15.5 \pm 0.5$ Å and $\gamma = 75 \pm 3°$. The angle θ between one diagonal of either 'α' or 'β' $F_{16}CuPc$ molecules and the molecular chain direction is $30 \pm 2°$, as labelled, similar to that on Ag(1 1 1) or Bi-$\sqrt{3}$. $F_{16}CuPc$ deposited on EG on SiC(0 0 0 1) exhibits similar packing to that on HOPG, as shown in figure 4(*b*). The molecular chain direction is aligned roughly with the C–C bond direction of the substrate [93]. The molecularly resolved STM image taken at RT in figure 4(*c*) reveals that $F_{16}CuPc$ on Cu(1 1 1) either assemblies into DMCs, similar to that on Ag(1 1 1), but along the NN directions on terraces [94], or forms the well-ordered pure α or β phase, as that on HOPG. One oblique unit cell of parameters $a = 14.5 \pm 0.5$ Å, $b = 14.5 \pm 0.5$ Å and $\gamma = 75 \pm 2°$ is indicated. Given the Cu(1 1 1) lattice constant of 2.55 Å, the 1st ML $F_{16}CuPc$ grows based on uniaxial point-on-line epitaxy with the substrate [94, 95].

Previous reports [96–98] of $F_{16}CuPc$ on Au(1 1 1) are inconsistent. In [96], the authors report that $F_{16}CuPc$ molecules at RT arrange into an oblique lattice with parameters $a = 15.1 \pm 0.8$ Å, $b = 14.5 \pm 0.8$ Å and $\gamma = 75 \pm 2°$. The molecular diagonal is tilted $51 \pm 3°$ with respect to the *b*-axis, which aligns with the NN directions of the substrate, as shown in figure 4(*d*). Six discrete rotational domains related by 30° are observed, as shown in the inserted LEED pattern [97]. In contrast, LT-STM measurements [98] reveal that $F_{16}CuPc$ self-assembles into commensurate molecular rows with the diagonals of $F_{16}CuPc$ along the crystallographic directions of Au(1 1 1), the same as that on Ag(1 1 1) [80]. More detailed experiments are needed to resolve such inconsistency. Nevertheless, by re-analysing the RT-STM results, if it is not the *b*-axis but the *a*-axis along the NNN direction, the diagonals of $F_{16}CuPc$ will align along the crystallographic directions of Au(1 1 1), as with the above-mentioned 3-fold symmetric substrates. Therefore, the enclosed angle between one diagonal of $F_{16}CuPc$ and *a*-axis, θ, is 30°. Consequently, γ is corrected to be $69 \pm 3°$.

2.4. $F_{16}CuPc$ on 4-fold surface

STM images in figure 5 display 1 ML $F_{16}CuPc$ on (*a*), (*b*) Bi(1 1 0) [81], (*c*) Au(1 0 0) and (*d*) Cu(1 0 0) [96], respectively, revealing that the $F_{16}CuPc$ molecules adopt a

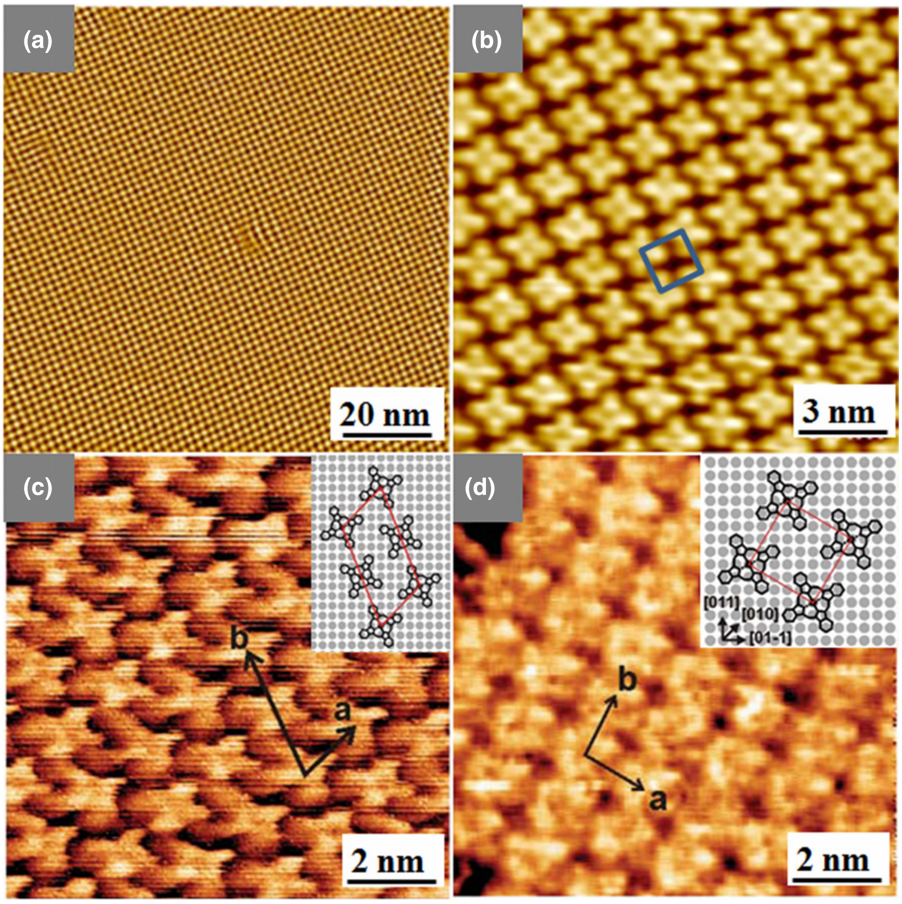

Figure 5. (*a*) large-scale ($V_T = 2.70$ V, $I_T = 0.1$ nA) and (*b*) corresponding zoomed-in ($V_T = 2.70$ V, $I_T = 0.1$ nA) STM images of 1 ML F_{16}CuPc on Bi(1 1 0) showing that F_{16}CuPc molecules assemble into a highly ordered square superstructure. (*c*), (*d*) STM image of 1 ML F_{16}CuPc on Au(1 0 0) (Cu(1 0 0)). The unit cell vectors *a* and *b* are indicated, respectively. The proposed models are shown as insets. (Figures (*a*) and (*b*) reprinted with permission from [81], copyright (2010) by the American Chemical Society; Figures (*c*) and (*d*) reprinted with permission from [96], copyright (2010) by American Institute of Physics.)

'lying-down' configuration on these substrates. Figure 5(*a*) shows that F_{16}CuPc molecules assemble into a highly ordered square superstructure with a lattice constant of $a = 15 \pm 1$ Å on Bi(1 1 0). The high-resolution STM image in figure 5(*b*) shows that all F_{16}CuPc molecules on Bi(1 1 0) have identical in-plane orientations, which can be attributed to the same 4-fold symmetry of Bi(1 1 0) and F_{16}CuPc. The intermolecular distance ($a = 15.0 \pm 1$ Å) does not fit any integer multiple of the unit cell ($\boldsymbol{a}_2 = 4.54$ Å, $\boldsymbol{b}_2 = 4.75$ Å) of Bi(1 1 0). Therefore, the structure is not commensurate with the substrate [95]. It suggests a relatively weak interfacial interaction between F_{16}CuPc and Bi(1 1 0), attributed to the semimetal nature of Bi(1 1 0). The intermolecular interaction between 4-fold symmetric F_{16}CuPc drives the molecules to adopt a square adsorption symmetry with the benzenoid portions interdigitated.

On Au(1 0 0), F_{16}CuPc forms a commensurate quasi-hexagonal structure with its oblique unit cell comprising two molecules of disparate azimuthal orientations, as shown in figure 5(*c*). Such a quasi-hexagonal superstructure is related to the surface reconstruction of Au(1 0 0) [96]. It is reported that the surface layer is compressed by 20% with a quasi-hexagonal atomic arrangement and a periodic corrugation along the [0 1 1] and [0 1 −1] directions [99, 100]. One molecular diagonal is $65 \pm 3°$ off the high symmetry [0 1 1] or [0 1 −1] directions. The unit cell parameters are $a = 16.8 \pm 1$ Å, $b = 30.8 \pm 0.5$ Å and $\gamma = 65 \pm 3.5°$, and the *a*-axis is oriented along the [0 1 0] or [0 0 1] directions. A proposed model is shown as an inset. On Cu(1 0 0), F_{16}CuPc forms commensurate overlayers in 2D [101], which can be described by a matrix of $\begin{pmatrix} 5 & 3 \\ -3 & 5 \end{pmatrix}$, as shown in figure 5(*d*). The unit cell is square, with a lattice parameter of 14.8 ± 1 Å. Each F_{16}CuPc molecule rotates by $\sim 13.5°$ relative to the row direction to avoid steric repulsion. The corresponding schematic drawing of the proposed structural model is shown as an inset, where all the F_{16}CuPc molecules have identical in-plane orientations.

On 3-fold symmetric substrates such as Cu(1 1 1), Ag(1 1 1), Au(1 1 1), Bi-$\sqrt{3}$, HOPG, both diagonals of the square-like F_{16}CuPc are along the crystallographic directions of the substrates with the molecular π-plane parallel to the substrates, due to the influence of the substrates. F_{16}CuPc molecules in similar configurations arrange themselves into 1D molecular chains along the crystallographic directions. Due to the mirror symmetry along the molecular chain direction, the chains with molecules in two equivalent configurations (α and β) are usually observed on the same terrace. Resulting from

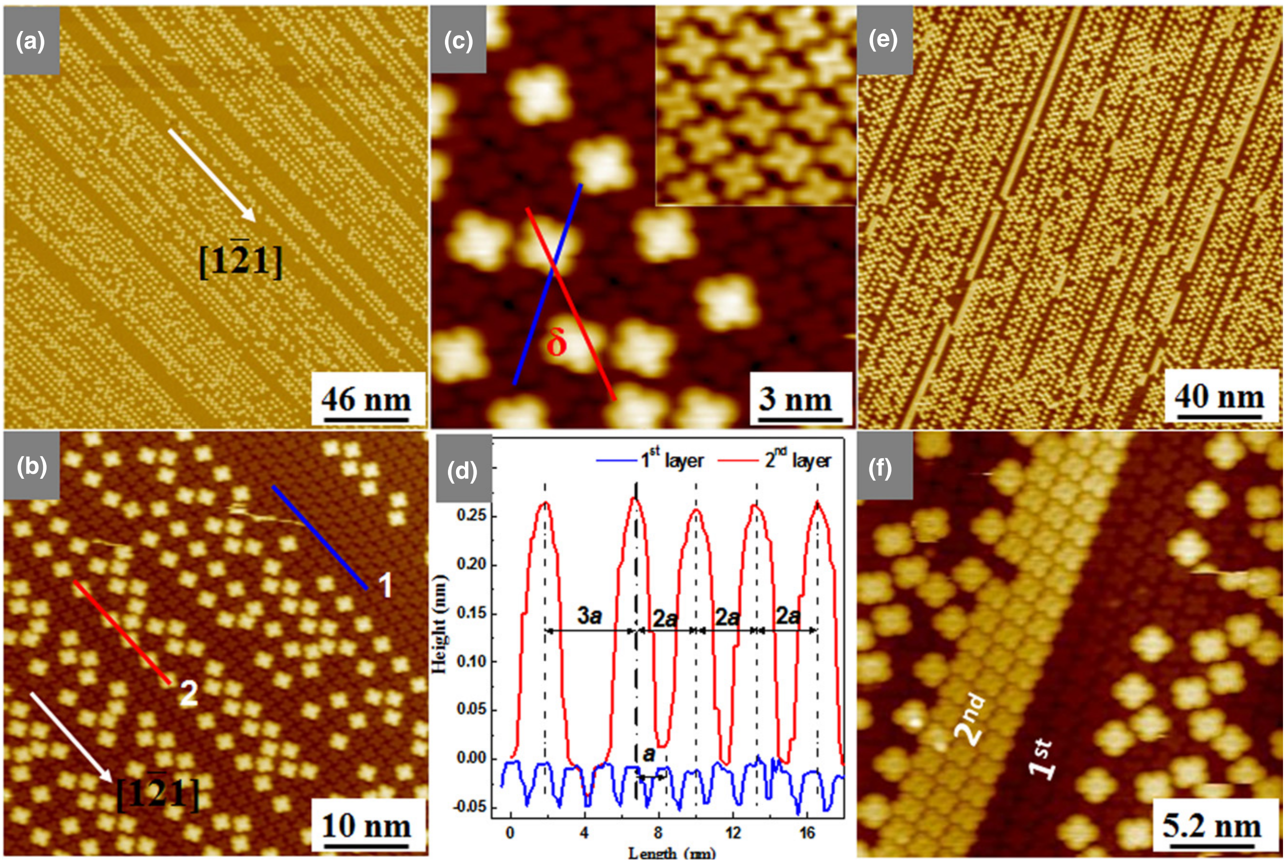

Figure 6. Initial growth of the 2nd ML F_{16}CuPc on Ag(1 1 1). (*a*) Large-scale STM image ($V_T = 2.90$ V, $I_T = 0.1$ nA) and (*b*) corresponding close-up ($V_T = 2.80$ V, $I_T = 0.1$ nA) of around 0.2 ML more F_{16}CuPc molecules deposited on one ML F_{16}CuPc covered Ag(1 1 1) surface. (*c*) Enlarged STM image from panel (*b*) showing the relative rotation between molecules in the first two layers. (*d*) Line profiles taken along lines 1 (blue) and 2 (red) in panel (*b*). the intermolecular distance of molecules in the 1st ML is defined as '$\boldsymbol{a}$'. (*e*) Large-scale ($V_T = 2.60$ V, $I_T = 0.1$ nA) and (*f*) corresponding zoomed-in ($V_T = 2.80$ V, $I_T = 0.1$ nA) STM images of the close-packed 2nd ML F_{16}CuPc on Ag(1 1 1). (Figures reprinted with permission from [80], copyright (2008) by the American Chemical Society.)

the delicate balance between molecule–molecule interactions and molecule–substrate interactions, the 1D F_{16}CuPc chains pack in pure α (β) phase or mixed α and β phase. On 4-fold symmetric substrates such as Bi(1 1 0) and Cu(1 0 0), F_{16}CuPc molecules form well-ordered 2D overlayers with a square unit cell and are packed in an interleaved fashion, with the benzenoid portions interdigitated, with all the molecules having identical in-plane orientation. The quasi-hexagonal surface reconstruction of Au(1 0 0) may cause the alternative $\alpha\beta$-like superstructure.

3. The growth of the 2nd ML F_{16}CuPc

Many MPcs' bulk packing structures have been determined from x-ray diffraction measurements [102]. The most prevalent single crystal structures are designated α or β phase depending on the type of intermolecular stacking between the Pc macrocycles [103–105]. For the 2nd ML, MPcs tend to aggregate into close-packed islands, for example, CoPc [106] and FePc [49] on Au(1 1 1), FePc on Cu(1 1 1) [107] and CuPc on Ag(1 1 1) [84], where the molecules adopt a non-planar configuration. While CoPc molecules in the 2nd ML stay exactly on top of those in the 1st ML [106], FePc molecules in the 2nd ML slightly shift along the diagonal of the unit cell of those in the 1st ML [49]. Some isolated molecules can also be observed, which is used to identify the relationship between molecules in the first two layers. CoPc is preferentially located almost vertically above a 1st ML CoPc without any obvious rotation, although occasionally a CoPc molecule may adsorb at the hollow site among four neighbouring 1st ML CoPc molecules [108]. In summary, the 2nd ML MPcs adopt different adsorption configurations relative to those in the 1st ML, depending on the interlayer intermolecular π interactions. In the following subsections, the arrangement of F_{16}CuPc in the 2nd ML will be discussed in detail.

3.1. 2nd ML F_{16}CuPc on Ag(1 1 1)

The initial growth of the 2nd ML starts after the completion of the 1st ML, but is considerably different from that of the 1st ML. Instead of forming close-packed single-layered islands, isolated F_{16}CuPc molecules align along the DMC directions, i.e. the NNN directions of Ag(1 1 1), forming 1D molecular dot chains, as shown in figure 6(*a*). The corresponding close-up is shown in figure 6(*b*). Similar to the 1st ML where the F_{16}CuPc molecules in the neighbouring DWCs adopt different in-plane orientations, those in the 2nd ML also possess two different in-plane orientations. The isolated $F_{16}CuPc$ molecules preferentially adsorb at the atop sites of molecules in the 1st ML with the molecular π-planes parallel to Ag(1 1 1). This confirms the π–π stacking between the first two layers $F_{16}CuPc$.

The submolecularly resolved STM image in figure 6(*c*) shows the positional relationship between the first two layers of $F_{16}CuPc$ molecules. The inset highlights the molecular arrangement in the underlying 1st ML. The blue (red) line indicates one diagonal of the molecule in the 1st (2nd) ML. Close inspection reveals that the four lobes of the upper molecule are not stacked directly above the underlying 1st layer molecules (on-top site), but are rotated by an angle, δ, of about 45°. This can be understood in terms of minimization of steric repulsion. Such a configuration is often observed for double-decker molecules [27, 28]. The line profiles in figure 6(*d*) show that the intermolecular distance between the neighbouring isolated $F_{16}CuPc$ molecules (the upper red line) along the [1 −2 1] direction of Ag(1 1 1) is double (2*a*) or triple (3*a*) of the intermolecular distance (*a*) of the 1st ML along the same direction (the lower blue line). Larger intermolecular separations of integer multiples of *a* can also be found. For the rotated $F_{16}CuPc$ molecules in the 2nd ML, the projected molecular length along the [1 −2 1] direction is larger than *a* as can be seen in the geometrical rotation of a square. It precludes the possibility of two rotated $F_{16}CuPc$ molecules being adsorbed on top of two adjacent molecules in the 1st ML along the [1 −2 1] direction. Otherwise, significant overlapping between these two rotated molecules would occur, hence inducing large repulsive forces between them. A way to reduce such assumed repulsion is to rotate the molecules in the 2nd ML, which will increase the interfacial repulsion because of more overlapping between the benzenoid portions in the two ML. The absence of such arrangement suggests that the interfacial repulsion is stronger than the in-plane one. This is consistent with the line profile measurements. The minimum intermolecular distance between the isolated $F_{16}CuPc$ in the 2nd ML along the [1 −2 1] direction is 2*a*, not *a*. The interlayer separation is measured to be 2.7 ± 0.1 Å, slightly smaller than the previously reported intermolecular distance of co-facially oriented $F_{16}CuPc$ molecules of around 3.1 Å, determined by the x-ray diffraction measurements. This discrepancy is attributed to the fact that the STM image is a convolution of both electronic and geometric properties of the surface.

At higher coverage, the incoming $F_{16}CuPc$ molecules will either stack on top of these isolated 2nd ML molecules to form the 3rd ML or induce a structural rearrangement of the isolated molecules to a densely packed 2nd ML. In our experiments, we observe the latter. Densely packed molecular nanoribbons along the [1 −2 1] direction are formed as shown in figure 6(*e*). Figure 6(*f*) displays a nanoribbon in the 2nd ML consisting of three molecular rows with isolated molecules located nearby. It is worth noting that all $F_{16}CuPc$ molecules in this three-molecule-wide nanoribbon adopt the same in-plane orientation and a π–π stacking along the direction perpendicular to the molecular plane. The interlayer electrostatic repulsion force can therefore be reduced by a small lateral displacement and molecular in-plane rotation between the 1st and 2nd ML molecules. Such π–π stacking between the first two ML is mainly stabilized through the interlayer dispersion forces. Upon increasing the coverage to 2 ML, the 2nd ML is fully saturated. The growth process of the 2nd ML is dominated by the intermolecular repulsion, similar to that of the 1st ML CuPc on Ag(1 1 1) [46, 47], but different from that of the 1st ML $F_{16}CuPc$ on Ag(1 1 1).

3.2. 2nd ML $F_{16}CuPc$ on HOPG and Bi-$\sqrt{3}$

The 2nd ML $F_{16}CuPc$ on HOPG aggregates into large islands with few vacancy defects, as shown in figure 7(*a*). Figure 7(*b*) is a close-up of the island edge, enlarged from the region highlighted by the rectangle in figure 7(*a*). The molecules in the 2nd ML also lie flat, attributed to interlayer π–π interactions. The most notable difference in the growth behaviours of the 1st and 2nd ML lies in their in-plane molecular orientation. As indicated by the blue arrows in figure 7(*b*), the molecules in the 2nd ML adopt the same in-plane orientation. Inspection reveals that if the molecules in the 1st and 2nd ML are in the inconsistent in-plane orientations, the ones in the 2nd ML will reside at atop sites of those in the 1st ML; if they are in the consistent in-plane orientations, the ones in the 2nd ML will shift laterally along the molecular row direction of those in the 1st ML, as indicated by the two lines in figure 7(*b*). Such configurations can minimize the repulsion between molecules in the 1st and 2nd ML efficiently. Similar packing for $F_{16}CuPc$ on Bi-$\sqrt{3}$ has also been observed, as shown in figures 7(*c*) and (*d*).

3.3. 2nd ML $F_{16}CuPc$ on Bi(1 1 0)

The initial growth behaviour of the 2nd ML $F_{16}CuPc$ on Bi(1 1 0) is shown in the typical LT-STM image in figure 8(*a*). The impinging $F_{16}CuPc$ initially adsorb as isolated molecules randomly distributed on top of the 1st ML. The corresponding high-resolution image in figure 8(*b*) reveals that the four lobes of the molecules in the 2nd ML are rotated by $\theta \approx 45°$ relative to those in the 1st ML, the same as on Ag(1 1 1). By increasing the $F_{16}CuPc$ coverage to 1.4 ML, the molecules in the 2nd ML form a short-range ordered ($\sqrt{2} \times \sqrt{2}$R45°) superstructure with respect to the 1st ML, as shown in figure 8(*d*). The intermolecular distance between the 2nd ML $F_{16}CuPc$ molecules is measured to be 2.0 nm, which is significantly larger than the vdW radii of $F_{16}CuPc$ [71].

Increasing the $F_{16}CuPc$ coverage above 1.5 ML induces a structural rearrangement in the 2nd ML. The ($\sqrt{2} \times \sqrt{2}$R45°) superstructure gradually transforms into a close-packed phase at 2 ML coverage. Figure 8(*e*) represents a typical molecularly resolved STM image of the close-packed 2nd ML. As marked by the red square in figure 8(*e*), the 2nd ML has a 4-fold symmetric unit cell with intermolecular distance of 15.0 Å, identical to that of the 1st ML. The 2nd ML possesses the same in-plane orientation as the 1st ML, but $F_{16}CuPc$ molecules in the 2nd ML are laterally displaced by about 2.0 Å with respect to those in the 1st ML, as marked by the dashed line in the inset. A similar growth behaviour of CoPc on Cu(1 0 0) has been reported [99]. The molecular

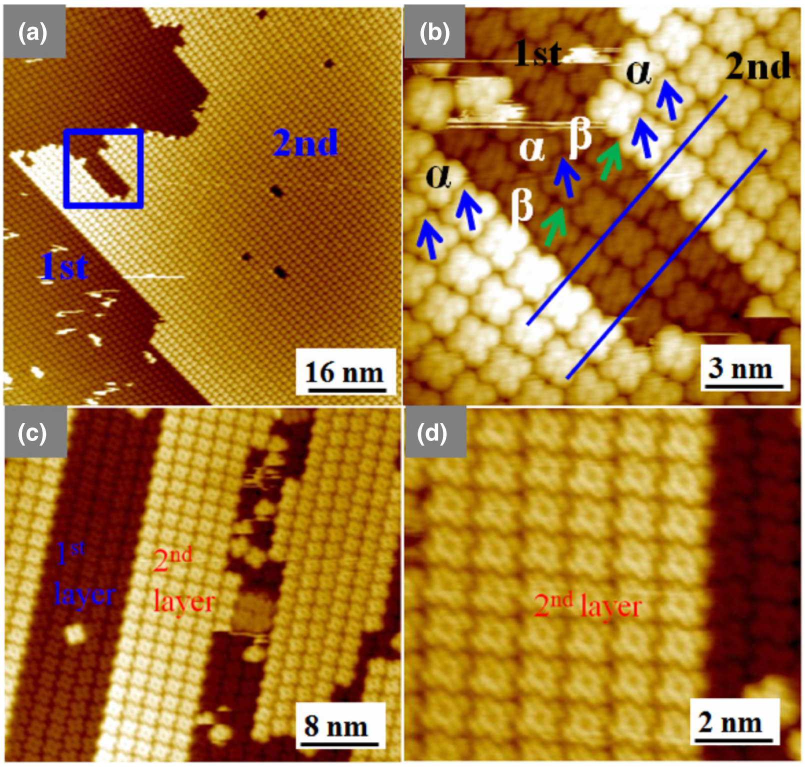

Figure 7. Growth of the 2nd ML $F_{16}CuPc$ on HOPG and Bi-$\sqrt{3}$. (*a*) STM images of 1.6 ML $F_{16}CuPc$ ($V_T = 2.50$ V, $I_T = 0.1$ nA) and (*b*) its corresponding close-up ($V_T = 2.50$ V, $I_T = 0.1$ nA) at the island edge, as marked by a rectangle in panel (*a*). The arrows indicate the molecular in-plane orientation. The two lines highlight the positional relationship of the 2nd ML molecules related to the 1st ML one. (*c*) Large-scale and (*d*) the corresponding zoomed-in STM images ($V_T = 2.53$ V, $I_T = 0.1$ nA) of $F_{16}CuPc$ on Bi-$\sqrt{3}$. (Figures (*a*) and (*b*) reprinted with permission from [82], copyright (2009) by the Springer; Figures (*c*) and (*d*) reprinted with permission from [81], copyright (2010) by the American Chemical Society.)

dynamics snapshots of the rotated and slipped 2nd ML clearly reproduce our STM observations, as shown in figures 8(*c*) and (*f*) [81].

The growth processes of the 2nd ML $F_{16}CuPc$ on 3-fold substrates depend on the choice of the substrates. On Ag(1 1 1), the growth process is dominated by intermolecular repulsion. The 2nd ML $F_{16}CuPc$ molecules preferentially adsorb on top of those in the 1st ML and rotate $\sim 45^\circ$ with respect to the underlying molecules, forming molecular dot chains along the NNN directions. Upon increasing the coverage $F_{16}CuPc$ insets between two isolated molecules to form nanoribbons along the NNN directions and then to form a close-packed 2D ordered molecular layer. On HOPG or Bi-$\sqrt{3}$, the growth process is dominated by the attractive intermolecular interaction. The incoming molecules aggregate into single-layered 2D islands. They either adsorb at the atop site of the underlying molecules if their in-plane orientations are different or shift laterally along the molecular chain direction off the atop sites if their in-plane orientations are identical. Thus two configurations can minimize the intermolecular repulsion effectively. On 4-fold Bi(1 1 0), the growth process is dominated by repulsive interaction between in plane molecules. The incoming molecules randomly reside on the atop sites, in the same out-of-plane configuration as that on Ag(1 1 1). Upon increasing coverage, phase transition from $\sqrt{2} \times \sqrt{2}$R45° to close-packed layer takes place.

4. CuPc on organic molecule pre-covered surfaces

4.1. CuPc on PTCDA-HOPG

The high-resolution STM image of 1 ML CuPc on HOPG in figure 9(*a*) clearly displays the typical CuPc intramolecular structure. The centre Cu atom appears as a dark hole. It is surrounded by eight bright spots, which arise from the two C atoms in the four pyrrole units, as shown by the molecular structure of CuPc in the inset. The outermost bright dots are attributed to the periphery benzene rings in CuPc [89]. PTCDA monolayer adopts an ordered in-plane herringbone arrangement with the extended π-plane oriented parallel to the HOPG surface with a rectangular unit cell of ~ 1.1 nm $\times$ 2.2 nm, due to the formation of multiple in-plane hydrogen bonds between neighbouring PTCDA [51, 110], as shown in the upper-right corner of figure 9(*c*). The multiple intermolecular hydrogen bonding ensures the structural rigidity of the PTCDA monolayer during the growth of organic adlayers. Figure 9(*b*) shows a stripe-like single-layered CuPc island on ML PTCDA on HOPG. The dislocation lines in the CuPc layer are separated by an average distance of 13 ± 1 nm, attributed to the lattice mismatch between CuPc and the underlying PTCDA. The line profile (not shown here) across the domain boundary of CuPc layer reveals that the average height of the CuPc layer is about 0.3 nm. As such, the CuPc molecules assemble as a single layer with their molecular planes parallel to the surface. Figure 9(*c*)

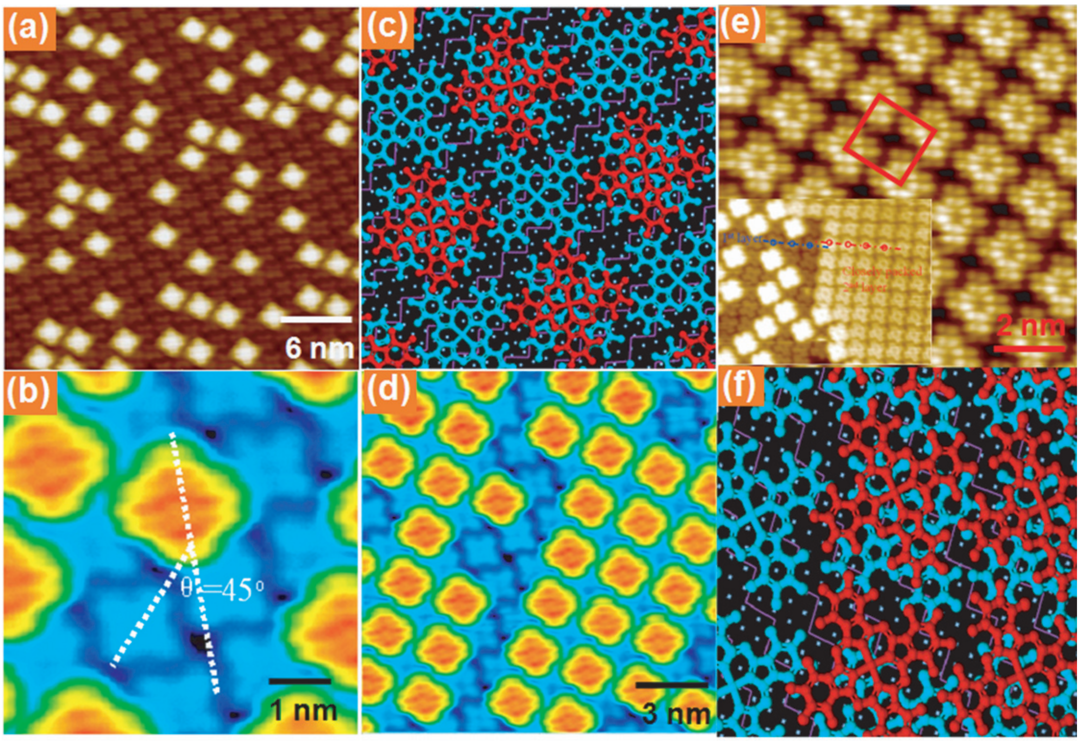

Figure 8. Initial growth of the 2nd ML F_{16}CuPc on Bi(1 1 0). (*a*) ($V_T = 2.82$ V, $I_T = 0.1$ nA) At coverage of 1.2 ML, F_{16}CuPc molecules absorb as isolated molecules, randomly distributed on the 1st ML; (*b*) molecularly resolved STM image ($V_T = 2.82$ V, $I_T = 0.1$ nA) showing that the in-plane orientation of the 2nd ML molecules are rotated by an angle of $\theta \approx 45°$ with respect to those in the 1st ML; (*c*) The corresponding snapshot of the MD simulation at 500 ps; (*d*) STM image ($V_T = 2.53$ V, $I_T = 0.1$ nA) of 2nd ML molecules form a short-range $(\sqrt{2} \times \sqrt{2})$ R45° superstructure with respect to the 1st ML at a coverage of 1.4 ML. (*e*) High-resolution STM image ($V_T = 2.70$ V, $I_T = 0.1$ nA) of the close-packed 2nd ML F_{16}CuPc on Bi(1 1 0); a unit cell is highlighted by the red square; An STM image ($V_T = 2.70$ V, $I_T = 0.1$ nA) with the 1st and 2nd layer molecular structures simultaneously resolved is inserted; (*f*) The corresponding snapshot of the MD simulation at 500 ps. (Figures reprinted with permission from [81], copyright (2010) by the American Chemical Society.)

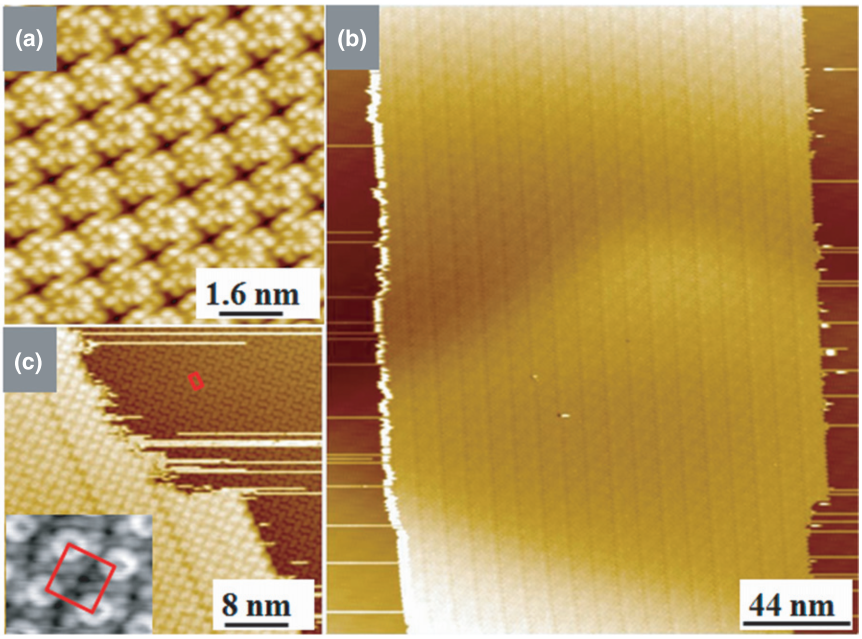

Figure 9. CuPc on PTCDA pre-covered HOPG. (*a*) submolecularly resolved STM image ($V_T = 1.50$ V, $I_T = 0.1$ nA) of 1 ML CuPc on HOPG. (*b*) Large-scale STM image ($V_T = 2.70$ V, $I_T = 0.1$ nA) and (*c*) close-up ($V_T = 2.70$ V, $I_T = 0.1$ nA) from single-layered CuPc islands on PTCDA covered HOPG. The inset in figure 9(*c*) highlights the intramolecular structure of CuPc on PTCDA. One square unit cell of CuPc is indicated. The rod-like PTCDA molecules arrange themselves into a herringbone structure. One unit cell comprising two PTCDA molecules is indicated by a rectangle. (Figure (*a*) reprinted with permission from [83b], copyright(2007) by American Institute of Physics; Figure (*c*) amended and reprinted with permission from [83a], copyright(2008) by the American Chemical Society.)

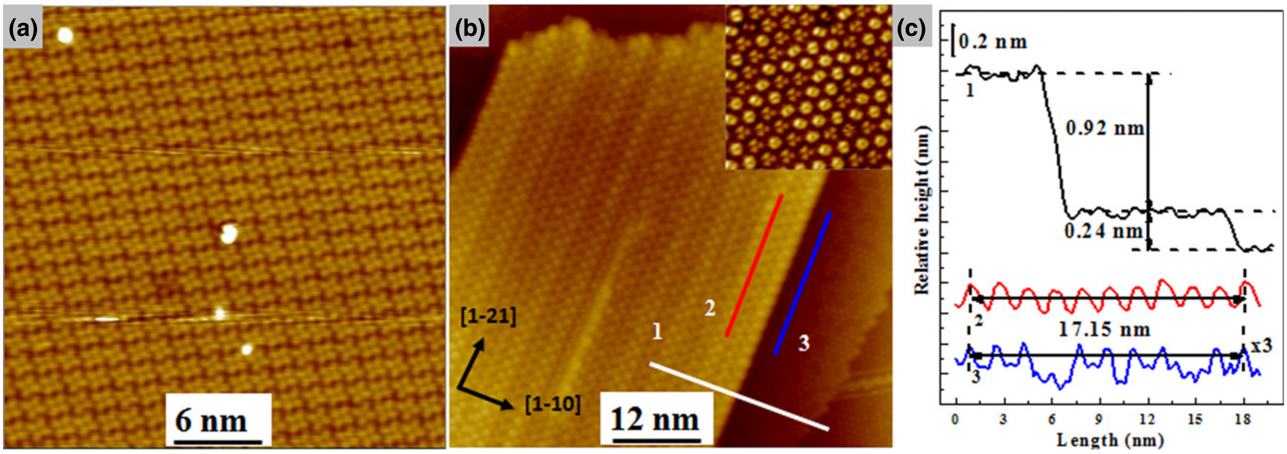

Figure 10. STM images of CuPc (*a*) ($V_T = -1.50$ V, $I_T = 0.1$ nA) on Ag(1 1 1) and (*b*) ($V_T = -2.13$ V, $I_T = 0.1$ nA) on C_{60}/Ag(1 1 1). The inset in panel (*b*) (10 nm × 10 nm, $V_T = -2.00$ V, $I_T = 0.1$ nA) shows the molecular packing of C_{60} on Ag(1 1 1). (*c*) line profiles taken along the lines 1, 2 and 3, as marked in (*b*), respectively. (Figures reprinted with permission from [84], copyright(2009) by American Institute of Physics.)

displays the corresponding high-resolution STM image of the CuPc single layer on PTCDA with detailed internal molecular structure. CuPc adopts a typical supramolecular arrangement with 4-fold symmetry. As shown in the inset, the centre Cu atom appears as a dark hole. The rectangle in the inset highlights the 1.5 × 1.5 nm^2 unit cell of CuPc on PTCDA [111].

4.2. CuPc on C_{60}-Ag(1 1 1)

Figure 10(*a*) shows that CuPc lies flat on Ag(1 1 1) in a rectangular close-packed configuration at one ML coverage. Figure 10(*b*) shows that CuPc forms well-ordered single-layered islands on top of the hexagonally close-packed (hcp) C_{60} ML, as shown in the inset. The brighter stripes in figure 10(*b*) are moiré patterns induced by the lattice mismatch between CuPc and C_{60}. Clearly the stripes align along the [1 −2 1] direction of the underlying hcp C_{60} layer. Figure 10(*c*) shows three line profiles taken along line 1 (across the step edge of CuPc island), line 2 (along the CuPc molecular stripes) and line 3 (along the [1 −2 1] direction of the hcp C_{60} layer), as marked in figure 10(*b*). The measured large apparent height (∼0.92 nm) of the CuPc island suggests that the CuPc molecules stand up on C_{60} with a tilted configuration. Line profile 2 taken along the CuPc molecule-row direction reveals a periodicity of ∼1.72 nm, coincident with the lattice constant along the [1 −2 1] direction of the hcp C_{60}. The observed standing-up orientation of the CuPc densely packed single-layered islands on C_{60} can be stabilized through the intermolecular π–π interaction between the neighbouring CuPc molecules, as well as the interfacial interaction involving the attractive C–H$\cdots\pi$ electrostatic intermolecular interaction between CuPc and the underlying C_{60} [84].

5. Conclusion

In summary, the growth behaviours of the 1st and 2nd ML F_{16}CuPc on selected 3-fold and 4-fold symmetric substrates have been reviewed. It is found that the growth behaviours of F_{16}CuPc are strongly affected by the underlying substrate. On 3-fold symmetric substrates, both diagonals of the square-like F_{16}CuPc lie along the crystallographic directions of the substrates with the molecular π-plane parallel to the substrates. The intermolecular attractions drive the 1st ML F_{16}CuPc into 2D single-layered islands, comprising 1D molecular chains with/without identical in-plane orientations. On 4-fold symmetric substrates, F_{16}CuPc molecules form well-ordered 2D overlayers with a square unit cell packed in an interleaved fashion, with the benzenoid portions interdigitated; all molecules have identical in-plane orientations. For F_{16}CuPc molecules in the 2nd ML, the impinging F_{16}CuPc molecules either adsorb as isolated molecules or aggregate into 2D islands, dependent on the relative out-of-plane molecular configurations, which can minimize the out-of-plane intermolecular repulsion.

The systematical investigations on the growth behaviours of F_{16}CuPc by LT-STM can provide a better understanding and control of the supramolecular packing and adsorption configurations at the molecular level. It offers the possibility of tailoring the electronic and physicochemical properties required for the fabrication of organic molecules based devices, such as OLEDs, OFETs, OPVs and organic spintronics.

Acknowledgment

Authors acknowledge the support from NRF-CRP Grant R-143-000-360-281 ‘Grapene and related materials and devices’.

References

[1] Forrest S R 2004 *Nature* **428** 911
[2] Chua L L, Zaumseil J, Chang J F, Ou E C W, Ho P K H, Sirringhaus H and Friend R H 2005 *Nature* **434** 194
[3] Forrest S R 2005 *MRS Bull.* **30** 28
[4] Yang F, Shtein M and Forrest S R 2005 *Nature Mater.* **4** 37
[5] Muccini M A 2006 *Nature Mater.* **5** 605

[6] Rogers J A 2001 *Science* **291** 1502
[7] Dimitrakopoulos C D and Malenfant P R L 2002 *Adv. Mater.* **14** 99
[8] Burghard M, Klauk H and Kern K 2009 *Adv. Mater.* **21** 1
[9] Koch N 2007 *ChemPhysChem* **8** 1438
[10] Forrest S R 2003 *Org. Electron.* **4** 45
[11] Dediu V A, Hueso L E, Bergenti I and Taliani C 2009 *Nature Mater.* **8** 707
[12] Ishii H, Sugiyama K, Ito E and Seki K 1999 *Adv. Mater.* **11** 605
[13] (a) Kahn A, Koch N and Gao W Y 2003 *J. Polym. Sci.* B **41** 2529
(b) Cahen C and Kahn A 2003 *Adv. Mater.* **15** 271
[14] Fang L, Park J Y, Ma H, Jen A K Y and Salmaron M 2007 *Langmuir* **23** 11522
[15] Osikowicz W, de Jong M P and Salaneck W R 2007 *Adv. Mater.* **19** 4213
[16] Chen W, Qi D C, Huang H, Gao X Y and Wee A T S 2011 *Adv. Funct. Mater.* **21** 410
[17] Koch N, Duhm S, Rabe J P, Vollmer A and Johnson R L 2005 *Phys. Rev. Lett.* **95** 237601
[18] de Boer B, Hadipour A, Mandoc M M, van Woudenbergh T and Bolm P W M 2005 *Adv. Mater.* **17** 621
[19] Khodabakhsh S, Sanderson B M, Nelson J and Jones T S 2006 *Adv. Funct. Mater.* **16** 95
[20] Chen W, Gao X Y, Qi D C, Chen S, Chen Z K and Wee A T S 2007 *Adv. Funct. Mater.* **17** 1339
[21] Chen W, Qi D C, Gao X Y and Wee A T S 2009 *Prog. Surf. Sci.* **84** 279
[22] Li L Q, Tang Q X, Li H X, Yang X D, Hu W P, Song Y B, Shuai Z G, Xu W, Liu Y Q and Zhu D B 2007 *Adv. Mater.* **19** 2613
[23] Gao L *et al* 2007 *Phys. Rev. Lett.* **99** 106402
[24] Tsukahara N *et al* 2009 *Phys. Rev. Lett.* **102** 167203
[25] Wackerlin C, Chylarecka D, Kleibert A, Muller K, Lacovita C, Nolting F, Jung Th A and Ballav N 2010 *Nature Commun.* **1** 61
[26] Komeda T, Isshiki H, Liu J, Zhang Y F, Lorente, Katoh K, Breedlove B K and Yamashita M 2011 *Nature Commun.* **2** 217
[27] Zhao A D *et al* 2005 *Science* **309** 1542
[28] Katoh K, Komeda T and Yamashita M 2010 *Dalton Trans.* **39** 4708
[29] Flechtner K, Kretschmann A, Steinruck H and Gottfried J M 2007 *J. Am. Chem. Soc.* **129** 12110
[30] Seufert K, Auwarter W and Barth J V 2010 *J. Am. Chem. Soc.* **132** 18141
[31] Lagally M G 1993 *Phys. Today* **11** 24
[32] Kowarik S, Gerlach A and Schreiber F 2008 *J. Phys.: Condens. Matter* **20** 1
[33] Kuhnle A 2009 *Curr. Opin. Colloid Interface Sci.* **14** 157
[34] Kowarik S, Gerlach A, Sellner S, Schreiber F, Cavalcanti L and Konovalov O 2006 *Phys. Rev. Lett.* **96** 125504
[35] Thayer G E, Sadowski J T, zu Heringdorf F M, Sakurai T and Tromp R M 2005 *Phys. Rev. Lett.* **95** 256106
[36] Crone B, Dodabalapur A, Lin Y Y, Filas R W, Bao Z, LaDuca A, Sarpeshkar R, Katz H E and Li W 2002 *Nature* **403** 521
[37] Zhao F, Harnisch F, Schröder U, Scholz F, Bogdanoff P and Herrmann I 2005 *Electrochem. Commun.* **7** 1405
[38] Craciun M F, Rogge S and, Morpurgo A F 2005 *J. Am. Chem. Soc.* **127** 12210
[39] Papageorgiou N, Salomon E, Angot T, Layet J M, Giovanelli L and Lay G L 2004 *Prog. Surf. Sci.* **77** 139.
[40] Han H, Zhang H J, Botters B, Qiao C, Mao H Y, Bin L, Li H Y, He P and Bao S N 2006 *J. Chem. Phys.* **124** 054716
[41] Song F *et al* 2007 *J. Phys.: Condens. Matter* **19** 136002
[42] Chen W, Huang H and Wee A T S 2008 *Chem. Commun.* **2008** 4276
[43] Wong S L, Huang H, Huang Y L, Wang Y Z, Gao X Y, Suzuki T, Chen W and Wee A T S 2010 *J. Phys. Chem.* C **114** 9356
[44] Matsubara R, Sakai M, Kudo K, Yoshimoto N, Hirosawa I and Nakamura M 2011 *Org. Electron.* **12** 195
[45] Komeda T, Isshiki H and Liu J 2010 *Sci. Technol. Adv. Mater.* **11** 054602
[46] Kroger I *et al* 2010 *New J. Phys.* **12** 083038
[47] Stadtmuller B, Kroger I, Reinert F and Kumpf C 2011 *Phys. Rev.* B **83** 085416
[48] Karacuban H, Lange M, Schaffert J, Weingart O, Wagner Th and Möller R 2009 *Surf. Sci.* **603** L39
[49] Cheng Z H, Gao L, Deng Z T, Liu Q, Jiang N,Lin X, He X B, Du S X and Gao H J 2007 *J. Phys. Chem.* C **111** 2656
[50] Huang H, Mao H Y, Chen Q, Yan X Z, Qian H Q, Zhang J H, Li H Y, He P M and Bao S N 2004 *Physica B: Condens. Matter* **352** 36
[51] Glockler K, Seidel C, Soukopp A, Sokolowski M, Umbach E, Bohringer M, Berndt R and Schneider W D 1998 *Surf. Sci.* **405** 1
[52] Swarbrick J C, Ma J, Theobald J A, Oxtoby N S, O'Shea J N, Champness N R and Beton P H 2005 *J. Phys. Chem.* B **109** 12167
[53] Tautz F S 2007 *Prog. Surf. Sci.* **82** 479
[54] Gustafsson J B, Zhang H M and Johansson L S O 2007 *Phys. Rev.* B **75** 155414
[55] Kilian L *et al* 2008 *Phys. Rev. Lett.* **100** 136103
[56] Grill L, Dyer M, Lafferentz L, Persson M, Peters M V and Hecht S 2007 *Nature Nanotechnol.* **2** 687
[57] Pfeiffer M, Leo K, Zhou X, Huang J S, Hofmann M, Werner A and Blochwitz-Nimoth J 2003 *Org. Electron.* **4** 89
[58] de Boer R W I, Stassen A F, Craciun M F, Mulder C L, Molinari A, Rogge S and Morpurgo A F 2005 *Appl. Phys. Lett.* **86** 262109
[59] Peumans P, Uchida S and Forrest S R 2003 *Nature* **425** 158
[60] Bouvet M 2006 *Anal. Bioanal. Chem.* **384** 366
[61] Cinchetti M, Heimer K, Wüstenberg J P, Andreyev O, Bauer M, Lach S, Ziegler C, Gao Y L and Aeschlimann M 2009 *Nature Mater.* **8** 115
[62] Kera S, Yamane H and Ueno N 2009 *Prog. Surf. Sci.* **84** 135
[63] Ueno N and Kera S 2008 *Prog. Surf. Sci.* **83** 490
[64] Rosei F, Schunack M, Naitoh Y, Jiang P, Gourdon A, Laegsgaard E, Stensgaard I, Joachim C and Besenbacher F 2003 *Prog. Surf. Sci.* **71** 95
[65] Bao Z, Lovinger A J and Brown J 1998 *J. Am. Chem. Soc.* **120** 207
[66] Klauk H, Zschieschang U, Pflaum J and Halik M 2007 *Nature* **445** 745
[67] Wang J, Wang H B, Yan X J, Huang H C and Yan D H 2005 *Appl. Phys. Lett.* **87** 093507
[68] Wang J, Wang H B, Yan X J, Huang H C, Jin D, Shi J W, Tang Y H and Yan D H 2006 *Adv. Funct. Mater.* **16** 824
[69] Lau K M, Tang J X, Sun H Y, Lee C S, Lee S T and Yan D H 2006 *Appl. Phys. Lett.* **88** 173513
[70] Osso J O, Schreiber F, Kruppa V, Dosch H, Garriga M, Alonso M I and Cerdeira F 2002 *Adv. Funct. Mater.* **12** 455
[71] Osso J O, Schreiber F, Alonso M I, Garriga M, Barrena E and Dosch H 2004 *Org. Electron.* **5** 135
[72] de Oteyza D G and Barrena E 2005 *Appl. Phys. Lett.* **87** 183504
[73] Güntherodt H J and Wiesendanger R (ed) 1992 *Scanning Tunneling Microscopy I: General Principles and Applications to Clean and Adsorbate-Covered Surfaces* 2nd edn (Berlin: Springer)

[74] Wiesendanger R and Güntherodt H J (ed) 1992 *Scanning Tunneling Microscopy II: Further Applications and Related Scanning Techniques* 2nd edn (Berlin: Springer)
[75] Wiesendanger R and Güntherodt H J (ed) 1993 *Scanning Tunneling Microscopy III: Theory of STM and Related Scanning Probe Methods* 2nd edn (Berlin: Springer)
[76] Gimzewski J K and Joachim C 1999 *Science* **283** 1683
[77] Huang H, Chen W, Chen S and Wee A T S 2008 *ACS Nano* **2** 2513
[78] Zhang H L, Chen W, Wang X S, Yuhara J and Wee A T S 2009 *Appl. Surf. Sci.* **256** 460
[79] McLeod I M, Dhanak V R, Matilainen A, Lahti M, Pussi K and Zhang K H L 2010 *Surf. Sci.* **604** 1395
[80] Huang H, Chen W and Wee A T S 2008 *J. Phys. Chem.* C **112** 14913
[81] Zhang K H L, Li H, Mao H Y, Huang H, Ma J, Wee A T S and Chen W 2010 *J. Phys. Chem.* C **114** 11234
[82] Huang Y L, Chen W, Chen S and Wee A T S 2009 *Appl. Phys.* A **95** 107
[83] (a) Chen W, Huang H, Chen S, Gao X Y and Wee A T S 2008 *J. Phys. Chem.* C **112** 5036
(b) Chen W, Huang H, Chen S, Chen L, Zhang H L, Gao X Y and Wee A T S 2007 *Appl. Phys. Lett.* **91** 114102
[84] Huang H, Chen W, Chen S, Qi D C, Gao X Y and Wee A T S 2009 *Appl. Phys. Lett.* **94** 163304
[85] Angot T, Salomon E, Papageorgiou N and Layet J M 2004 *Surf. Sci.* **572** 59
[86] Papageorgiou N, Ferro Y, Layet J M, Giovanelli L, Mayne A J, Dujardin G, Oughaddou H and Lay G L 2003 *Appl. Phys. Lett.* **82** 25
[87] Tekiel A, Goryl M and Szymonski M 2007 *Nanotechnology* **18** 475707
[88] Gopakumar T G, Lackinger M, Hackert M, Muller F and Hietschold M 2004 *J. Phys. Chem.* B **108** 7839
[89] Lu X, Hipps K W, Wang X D and Mazur U 1996 *J. Am. Chem. Soc.* **118** 7197
[90] Scudiero L, Hipps K W and Barlow D E 2003 *J. Phys. Chem.* B **107** 2903
[91] Wang Y F, Ge X, Manzano C, Kroger J, Berndt R, Hofer W A, Tang H and Cerda J 2009 *J. Am. Chem. Soc.* **131** 10400
[92] de Oteyza D G, Barrena E, Osso J O, Sellner S and Dosch H 2006 *J. Am. Chem. Soc.* **128** 15052
[93] Wang Y L *et al* 2010 *Phys. Rev.* B **82** 245420
[94] (a) Wakayama Y 2007 *J. Phys. Chem.* C **111** 2675
(b) Barrena E, de Oteyza D G, Dosch H and Wakayama Y 2007 *ChemPhysChem* **8** 1915
[95] Hooks D E, Fritz T and Ward M D 2001 *Adv. Mater.* **13** 227
[96] de Oteyza D G *et al* 2010 *J. Chem. Phys.* **133** 214703
[97] de Oteyza D G, Silanes I, Ruiz-Oses M, Barrena E, Doyle B P, Arnau A, Dosch H, Wakayama Y and Ortega J E 2009 *Adv. Funct. Mater.* **19** 259
[98] Chen L, Li H and Wee A T S 2009 *ACS Nano* **3** 3684
[99] Binning G K, Rohrer H, Gerber Ch and Soll E 1984 *surf. Sci.* **144** 321
[100] Gao X, Hamelin A and Weaver M J 1991 *Phys. Rev. Lett.* **67** 618
[101] Krauss T N, Barrena E, Dosch H and Wakayama Y 2009 *ChemPhysChem* **10** 2445
[102] Engel M K 2003 *The Porphyrin Handbook* vol 20, ed K M Kadish *et al* 2003 (San Diego, CA: Elsevier Science) p 1
[103] Hoshino A, Takenaka Y and Miyaji H 2003 *Acta Crystallogr.* B **59** 393
[104] Kera S, Casu M B, Bauchspie K R, Batchelor D, Schmidt Th and Umbach E 2006 *Surf. Sci.* **600** 1077
[105] de la Torre G, Claessens C G and Torres T 2007 *Chem. Commun.* **2007** 2000
[106] Takada M and Tada H 2004 *Chem. Phys. Lett.* **392** 265
[107] Scarfato A, Chang S H, Kuck S, Brede J, Hoffmann G and Wiesendanger R 2008 *Surf. Sci.* **602** 677
[108] Ge X, Manzano C, Berndt R, Anger L T, Khler F and Herges R 2009 *J. Am. Chem. Soc.* **131** 6096
[109] Guo Q M, Qin Z H, Zang K, Liu C D, Yu Y H and Cao G Y 2010 *Langmuir* **26** 11804
[110] Huang H, Chen S,Gao X Y, Chen W and Wee A T S 2009 *ACS Nano* **3** 3431
[111] Yim S, Heutz S and Jones T S 2003 *Phys. Rev.* B **67** 165308